Cooperative Aerial-Ground Vehicle Rendezvous with Integrated Obstacle Avoidance

Ghewa Masry[1], David Vieira[1], Rodolfo Orjuela[1], Thomas Meurer[2] and Michel Basset[1]

***Abstract*— This work addresses the integration of simultaneous obstacle avoidance for an Unmanned Aerial Vehicle (UAV) and an Unmanned Ground Vehicle (UGV) operating cooperatively to rendezvous at a predefined location. A distributed consensus-based architecture is proposed to guide the vehicles toward their designated rendezvous point. Additionally, a virtual force-based obstacle avoidance method is employed for both vehicles. A comparison is conducted with an existing control approach from the literature extended to incorporate obstacle avoidance. Simulation results are provided showing the ability of the presented controllers to achieve rendezvous while simultaneously avoiding obstacles.**

I. INTRODUCTION

Cooperation between Unmanned Aerial Vehicles (UAV) and Unmanned Ground Vehicles (UGV) has attracted significant research interest in recent years. The combination of their heterogeneous capabilities allows to leverage the best of both worlds, enabling UAV-UGV teams to accomplish complex tasks more efficiently than either vehicle alone. Motivated by the well-known limitation on the flight time of UAVs, an interesting application of the aerial-ground cooperation is the use of the UGVs as mobile recharging stations for the UAVs [1]. In such a scenario, the vehicles need to rendezvous at a location where the UAV can autonomously land on the UGV to recharge and complete the mission. While moving towards their meeting point, both vehicles may encounter obstacles along their paths. Therefore, it is important to ensure an efficient rendezvous while simultaneously avoiding obstacles.

Various approaches have been proposed in the literature to address the autonomous landing problem. Authors in [2] present a vision based landing system in which the UAV detects the landing platform and a controller based on a Control Barrier Function (CBF) and Control Lyapunov Function (CLF) is designed for tracking and landing. In [3], a gimbaled camera is used to track the platform and a linear Model Predictive Controller (MPC) is then proposed to plan and track the landing trajectory. Similarly in [4], the landing marker is detected and tracked and a MPC plans the landing trajectory which is then tracked by a cascade incremental nonlinear dynamic inversion (INDI) controller. In [5] UAV energy consumption constraints are considered, where the UAV must decide when and where to rendezvous considering its stochastic energy consumption. The rendezvous problem is formulated as a Chance-Constrained Markov Decision Process (CCMDP), which is then converted into a Constrained Markov Decision Process (CMDP) and solved using Linear Programming (LP). In a more recent work [1], the authors propose a more scalable bi-criteria approximation optimization algorithm to solve the risk-aware recharging rendezvous problem. Adopting a more model-based approach, [6] considers the planar dynamic models of both vehicles, a singular optimal rendezvous control problem is formulated using the Pontryagin's Maximum Principle (PMP). For landing of a fixed-wing UAV, in [7] a decoupled MPC strategy is introduced in which landing safety is ensured through danger zone UAV constraints. The rendezvous time and location are kept free and the MPC controller is decoupled into alignment and descent components which reduces computational complexity. Inspired by this, [8] proposes a model predictive trajectory planner based on the differential flatness property where the MPC is decoupled into horizontal and vertical planners. A leader-follower formation control approach based on sliding mode control (SMC) is presented in [9]. The UGV is the leader of the formation and the UAV follows it for tracking and landing. In [10], a joint decentralized controller is designed to land a quadrotor on a skid-steered UGV where each vehicle uses feedback linearization to simplify its dynamics but no exact meeting location was predefined for the two vehicles. Consequently, since feedback linearization reduces control complexity while accounting for the system's dynamic behavior, this approach is selected and extended here to include a predefined desired rendezvous location.

Moreover, none of the previously mentioned approaches consider obstacle avoidance for the vehicles in the rendezvous and autonomous landing problem. Authors in [11] present a path-following formation controller based on the virtual structure to guide the UAV-UGV formation, considering that the UAV should land on the UGV, while avoiding ground obstacles. An online path planning obstacle avoidance (OA) algorithm is presented to allow the formation, represented as a single virtual robot coinciding with the UGV, to choose the safest arc around detected obstacles. For UAV obstacle avoidance, [12] proposes an autonomous landing scheme in which landing markers are detected and a trajectory planning algorithm based on B-spline curve and A^* algorithm generates the collision-free path for the

This work is supported by the collaboration between the IRIMAS-UHA (France) and the KIT (Germany) in the framework of the Digital Process Engineering for Sustainable Materials and Energy.

[1]Institut de Recherche en Informatique, Mathématiques, Automatique et Signal (IRIMAS UR 7499), Université de Haute-Alsace, 68093 Mulhouse, France ghewa.masry@uha.fr, david.vieira-gois-fernandes@uha.fr, rodolfo.orjuela@uha.fr, michel.basset@uha.fr

[2]Karlsruhe Institute of Technology (KIT), 76131 Karlsruhe, Germany thomas.meurer@kit.edu

UAV. A similar approach is proposed in [13], where the UAV detects and estimates the landing target's position, then utilizes the A^* algorithm for path search. The initial path is further optimized using a Bernstein polynomial-based Bezier curve approach. In [14] the landing of multiple UAVs on moving UGVs and thus the inter-agent collision avoidance between UAVs is considered. A centralized control approach is presented with a landing CBF (LCBF) to ensure safe and precise landing on the UGVs and a Spherical CBF (SCBF) for collision avoidance. In summary, only a few works considering obstacle avoidance, for either vehicle, in the context of the rendezvous and autonomous landing problem exist in the literature.

In this work, the simultaneous obstacle avoidance and rendezvous problem is addressed. Initially, obstacle avoidance for both the UAV and UGV is integrated into the approach presented in [10] and extended to include a predefined meeting location. Due to their simplicity, potential field methods and repulsion forces are widely used for obstacle avoidance when dealing with solely ground or aerial vehicles. Therefore, the virtual force method presented in [15] is adopted for obstacle avoidance. Then, to enhance scalability, the joint controller in [10], which generates the control inputs for both vehicles, is replaced with two distributed consensus controllers, also integrating obstacle avoidance. In distributed consensus control, agents use their local and relative information to enable the group of agents to reach an agreement about their states [16]. Thus, the rendezvous problem, in which the vehicles must simultaneously reach a common meeting point, is considered as a direct application of distributed consensus control and the control inputs for the UGV and UAV are generated separately. It is assumed that only the UGV has knowledge of the predefined rendezvous location and both vehicles share their position information to move towards each other.

The rest of the paper is organized as follows. Section II presents a brief overview of the vehicle models. Then, the extended joint controller from [10] and the proposed consensus controllers with integrated obstacle avoidance, are presented in Section III. Simulation results and a comparison between the two approaches are presented in Section IV. Finally, the conclusion and future perspectives are given in Section V.

II. System Modeling

Subsequently, the vehicle models and their feedback linearization controllers are briefly presented. For further details, the reader is referred to [10].

A. Vehicle Models

1) UAV model: The quadrotor dynamic model has the following state vector [10]:

$$P_a = [x_a, \dot{x}_a, y_a, \dot{y}_a, z_a, \dot{z}_a, \phi_a, \dot{\phi}_a, \theta_a, \dot{\theta}_a, \psi_a, \dot{\psi}_a]^T \quad (1)$$

where $[x_a, y_a, z_a]^T$ is the position vector of the aerial vehicle, $[\dot{x}_a, \dot{y}_a, \dot{z}_a]$ are the velocities, $[\phi_a, \theta_a, \psi_a]$ are the Euler angles and $[\dot{\phi}_a, \dot{\theta}_a, \dot{\psi}_a]$ are the angular velocities.

Considering that gravity g and the total thrust U_1 are the only external forces acting on the quadrotor. The state space representation is given by:

$$\dot{P}_a = \begin{bmatrix} u_x \frac{U_1}{m} \\ \dot{y}_a \\ u_y \frac{U_1}{m} \\ \dot{z}_a \\ (\cos\phi_a \cos\theta_a)\frac{U_1}{m} - g \\ \dot{\phi}_a \\ \dot{\theta}_a\dot{\psi}_a\frac{I_y - I_z}{I_x} + \frac{l}{I_x}U_2 \\ \dot{\theta}_a \\ \dot{\phi}_a\dot{\psi}_a\frac{I_z - I_x}{I_y} + \frac{l}{I_y}U_3 \\ \dot{\psi}_a \\ \dot{\theta}_a\dot{\phi}_a\frac{I_x - I_y}{I_z} + \frac{l}{I_z}U_4 \end{bmatrix}, \quad (2)$$

where

$$u_x = \cos\phi_a \sin\theta_a \cos\psi_a + \sin\phi_a \sin\psi_a \quad (3a)$$

$$u_y = \cos\phi_a \sin\theta_a \sin\psi_a - \sin\phi_a \cos\psi_a. \quad (3b)$$

Herein, I_x , I_y, I_z are the inertia about the x, y and z body axes, respectively, and U_2, U_3, U_4 are the angular torques acting about the body roll axis, the pitch axis and the yaw axis, respectively. U_1, U_2, U_3 and U_4 represent the control inputs of the system. m is the mass and l is the distance from a motor to the center of mass (COM) of the quadrotor.

The altitude is feedback linearized into:

$$\ddot{z}_a = v_z, \quad (4)$$

by considering that:

$$U_1 = \frac{m}{\cos\phi_a \sin\theta_a}(v_z + g). \quad (5)$$

Finally, the quadrotor's positions can be treated as a linear double integrator with the virtual inputs v_a:

$$\begin{bmatrix} \ddot{x}_a \\ \ddot{y}_a \end{bmatrix} = v_a = \begin{bmatrix} v_{a,1} \\ v_{a,2} \end{bmatrix}, \quad (6)$$

where

$$\begin{bmatrix} \theta_a \\ \phi_a \end{bmatrix} = \frac{m}{U_1}\begin{bmatrix} \cos\psi_a & \sin\psi_a \\ \sin\psi_a & -\cos\psi_a \end{bmatrix} v_a. \quad (7)$$

As proposed in [10], an inner PD controller is used for the attitude control to track the desired generated values of θ_a and ϕ_a.

2) UGV model: The following kinematic model of a skid-steered ground vehicle is used [10] [17]:

$$\begin{bmatrix} \dot{x}_g \\ \dot{y}_g \\ \dot{\psi}_g \end{bmatrix} = \begin{bmatrix} \cos\psi_g & x_{ICR}\sin\psi_g \\ \sin\psi_g & -x_{ICR}\cos\psi_g \\ 0 & 1 \end{bmatrix} \begin{bmatrix} v_x \\ w \end{bmatrix}, \quad (8)$$

where $p_g = [x_g, y_g]^T$ is the position vector of the ground vehicle, ψ_g is the angle of the body-fixed frame in the global

coordinates, and x_{ICR} represents the x projection of the instantaneous center of rotation (ICR) of the vehicle into the body-fixed frame for which a constant approximation x_0 is used. Moreover, v_x and w denote the x-component of the translatory and the angular velocity, respectively.

The feedback linearization controller using input-output feedback linearization is presented by:

$$\begin{bmatrix} v_x \\ w \end{bmatrix} = \begin{bmatrix} \cos\psi_g & \sin\psi_g \\ \frac{\sin\psi_g}{x_0} & -\frac{\cos\psi_g}{x_0} \end{bmatrix} \begin{bmatrix} v_{g,1} \\ v_{g,2} \end{bmatrix}. \tag{9}$$

As a result, the ground vehicle's position can be treated as a linear single integrator:

$$\begin{bmatrix} \dot{x}_g \\ \dot{y}_g \end{bmatrix} = v_g = \begin{bmatrix} v_{g,1} \\ v_{g,2} \end{bmatrix}, \tag{10}$$

where $v_{g,1}$ and $v_{g,2}$ denote the virtual control inputs for the x and y positions of the UGV, respectively.

III. Consensus Control with Obstacle Avoidance

First, the virtual force method for obstacle avoidance from [15] is presented. Then, the joint controller from [10] is briefly presented with the desired rendezvous point and obstacle avoidance extensions. Finally, the proposed distributed consensus controllers are presented.

A. Virtual Force Method

The virtual force method presented in [15] is extended to also include the z-component as given by:

$$d_{io} = \sqrt{(x_i - x_o)^2 + (y_i - y_o)^2 + (z_i - z_o)^2} - r^2, \tag{11}$$

where d_{io} represents the distance from each vehicle to the obstacle, $p_i^{(3)} = [x_i, y_i, z_i]^T$ is the position of the vehicle i and $p_o^{(3)} = [x_o, y_o, z_o]^T$ is the position of the obstacle, which is considered to have a radius r. Noting that for the UGV, the z-component is considered to be fixed at $z_g = 0$.

It is assumed that the vehicles are equipped with sensors that can detect the obstacles and the positions of the obstacles are known. When the obstacle is detected, a repulsive force is generated:

$$u_{oa} = \left(\frac{F_{cr}}{d_{io}^2}\right)\left(\frac{1}{d_{io}} - \frac{1}{q}\right)\left(\frac{p_i^{(3)} - p_o^{(3)}}{d_{io}}\right). \tag{12}$$

Herein, F_{cr} is the repelling force constant and q is the safe distance. u_{oa} is inversely proportional to the square of the distance between the vehicle and the obstacle, so the repelling force intensifies as the vehicle gets closer to the obstacle. The term $\left(\frac{1}{d_{io}} - \frac{1}{q}\right)$ is to avoid the oscillation around the safe distance [15].

The term in (12) is then added to the control inputs for both vehicles, integrating obstacle avoidance.

B. Extended Joint Controller

The joint controller proposed in [10] is given by:

$$\begin{bmatrix} v_{g,i} \\ v_{a,i} \end{bmatrix} = -K_{jc,i} \begin{bmatrix} e_i \\ \dot{x}_a \end{bmatrix}, \ i \in \{1, 2\}. \tag{13}$$

where for $i = 1$, $e_1 = x_a - x_g$ represents the relative position error in the x-dimension, $v_{g,1}$ and $v_{a,1}$ are presented in (10) and (6), respectively, and $K_{jc,i} \in R^{2\times 2}$ is the gain matrix. Similarly for $i = 2$, $e_2 = y_a - y_g$ and $\dot{x}_a$ is replaced by $\dot{y}_a$ in (13).

This controller generates the control inputs for both vehicles based on driving the relative position errors to zero as well as the velocity of the aerial vehicle. On the other hand, the z-component is controlled separately through a PD controller, where the descent is only started when the vehicles are at a close distance from each other [10].

Extensions: The controller in (13) is extended to also consider a desired rendezvous point of position $p_r = [x_r, y_r]^T$. Since only the UGV is considered to know its location, the rendezvous component is added only to the UGV inputs as follows:

$$v_{g,1e} = v_{g,1} + K_{rx}(x_r - x_g) \tag{14a}$$

$$v_{g,2e} = v_{g,2} + K_{ry}(y_r - y_g), \tag{14b}$$

where K_{rx}, K_{ry} are the weights on the error between the UGV's position and that of the rendezvous point in the x and y directions respectively.

Moreover, for obstacle avoidance u_{oa} given in (12) is added and the total control input applied to each vehicle is then given by:

$$v_{i,t} = v_i + u_{oa}, \tag{15}$$

where v_i represents v_g and v_a for the ground and aerial vehicles with the joint controller respectively. The extended control architecture is given in Fig. 1.

C. Distributed Consensus Control

Two distributed consensus controllers are proposed to generate the control inputs for the UGV and UAV separately, instead of the single joint controller used earlier. Fig. 2 presents the new control architecture. It should be noted that with these new controllers, the previous inputs v_i in (6) and (10) are replaced by u_i presented in (17) and (16), respectively.

For the UGV, treated as a single integrator, the following control input is applied:

$$u_g = K_1(p_a - p_g) + K_2(p_r - p_g), \tag{16}$$

where the first term minimizes the relative error between the UAV with $p_a = [x_a, y_a]^T$ and the UGV while the second term drives the ground vehicle towards the predefined rendezvous point.

Meanwhile, for the UAV treated as a double integrator, the applied control input is given by:

$$u_a = K_3(p_g - p_a) - K_4\dot{p}_a, \tag{17}$$

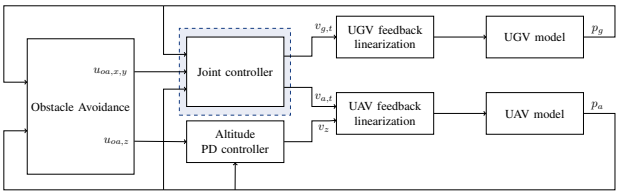

Fig. 1: Extended joint controller architecture.

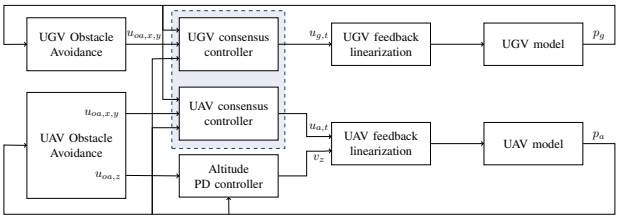

Fig. 2: Consensus controllers architecture.

in which, the first term is for the relative error minimization while the second term is to ensure that the velocity of the aerial vehicle, $\dot{p}_a$, converges to zero.

Herein, K_1, K_2, K_3 and K_4 are gains to be tuned, chosen as scalars, considering the trade-off between convergence time and control efforts.

As previously introduced, the obstacle avoidance control input (12) is added and the total control input applied to each vehicle is then:

$$u_{i,t} = u_i + u_{oa}, \tag{18}$$

where u_i represents u_g and u_a for the ground and aerial vehicles respectively.

A PD controller is also used for the descent as in [10].

Stability Analysis: Global stability is investigated to ensure that the relative error e and the rendezvous error e_r given by:

$$e = p_a - p_g, \quad e_r = p_r - p_g, \tag{19}$$

converge towards zero.

For the sake of simplicity, we assume that the vehicles do not get too close to the obstacles so the obstacle avoidance control input is neglected.

The first derivative of e is given by:

$$\dot{e} = \dot{p}_a - \dot{p}_g = v_a - K_1 e - K_2 e_r. \tag{20}$$

Moreover, for e_r the first derivative is:

$$\dot{e}_r = \dot{p}_r - \dot{p}_g = -K_1 e - K_2 e_r. \tag{21}$$

Taking the state vector: $\begin{bmatrix} e & e_r & \dot{p}_a \end{bmatrix}^T$ with $\ddot{p}_a = u_a$ from (17), the following state space representation is obtained along the x-axis (similarly along the y-axis):

$$\begin{bmatrix} \dot{e}_x \\ \dot{e}_{r,x} \\ \ddot{p}_{a,x} \end{bmatrix} = \begin{bmatrix} -K_1 & -K_2 & 1 \\ -K_1 & -K_2 & 0 \\ -K_3 & 0 & -K_4 \end{bmatrix} \begin{bmatrix} e_x \\ e_{r,x} \\ \dot{p}_{a,x} \end{bmatrix}. \tag{22}$$

For which, the characteristic polynomial can be written as:

$$\lambda^3 + (K_1 + K_2 + K_4)\lambda^2 + (K_3 + K_2 K_4 + K_4 K_1)\lambda + K_2 K_3. \tag{23}$$

Then, using pole placement, the polynomial in (23) is matched to a desired polynomial with specified eigenvalues. Given that the system of equations from (23) is underdetermined, K_4 is fixed for simplicity and the system is then solved through MATLAB's Symbolic Math Toolbox. Consequently, the values of K_1, K_2, and K_3 are deduced and the stability of the system is guaranteed. It is noteworthy that the eigenvalues are selected to achieve a desired behavior, compromising between the settling time and the control effort.

IV. Simulation Results

The presented controllers to deal with the rendezvous problem with a predefined rendezvous point and integrated obstacle avoidance are implemented in MATLAB, including the feedback linearizing controllers as well as the nonlinear models given in (2) and (8). The initial conditions for the ground and aerial vehicles are $p_{g0} = [0, 1]^T$ and $p_{a0}^{(3)} = [5, 4, 5]^T$ respectively.

The desired rendezvous point is set as $p_r = [5, 2, 0]^T$. Noting that the aerial vehicle is considered to land at $z = 0.5$ m.

A. Performance Metrics

The landing time is recorded when the UAV is considered to have landed on the UGV, which is when the position error is less than 1 cm and its altitude is $z = 0.5$ m. The total control effort generated by the controllers, for the UAV and UGV separately, is calculated by:

$$u_T = \int_0^T \left(u_{i_x}^2 + u_{i_y}^2 \right) dt. \tag{24}$$

B. Scenario 1: Two obstacles

Two obstacles with positions $p_{o1}^{(3)} = [1.5, 1.6, 0]^T$ and $p_{o2}^{(3)} = [3.5, 3, 5.6]^T$, are considered to be on the paths of the ground and aerial vehicles, respectively.

The controller parameters are selected to compromise between the convergence time and the control effort as follows: $K_1 = 0.03$, $K_2 = 0.034$, $K_3 = 0.04$, $K_4 = 0.2$ and for the joint controller extension $K_{jc,i}$ is the same as in [10] and $K_{rx} = K_{ry} = 0.045$. For the altitude PD controller, the proportional gain is $k_p = 0.02$ and the derivative gain is $k_d = 0.48$. For the virtual force method, $F_{cr} = 0.03$, $q = 1$, and $r = 0.2$ m for all obstacles.

The 3D trajectories followed by the UGV and UAV are presented in Fig. 3 and Fig. 4, which demonstrate the results from the joint controller and the consensus controllers respectively. It is shown that both approaches are capable of successfully avoiding the obstacles when the vehicles enter their detection zones (dashed circles), and rendezvous at the desired point. The significant difference in the UGV trajectories can be related to the sensitivity to controller gains, where converging to the rendezvous point or to meet the UAV can be prioritized. This is also noted in Fig. 5, where it can be seen that the UGV travels a shorter distance with the consensus controller than with the joint one. Conversely, the UAV travels a slightly greater distance.

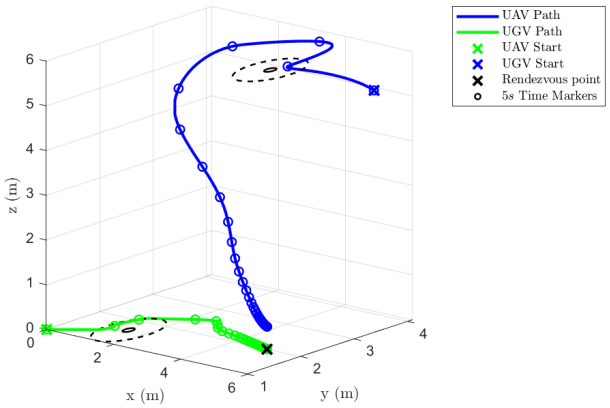

Fig. 3: Joint controller 3D trajectories of the UAV and UGV with two obstacles.

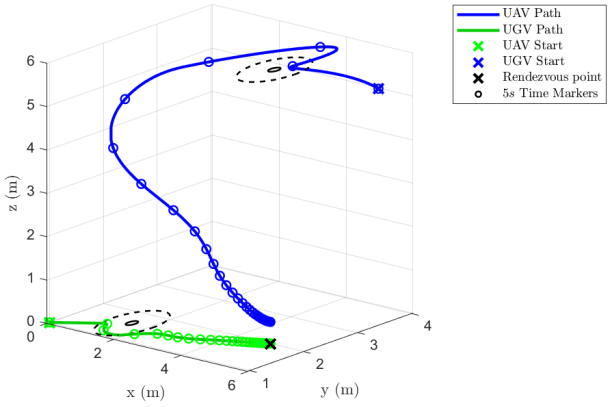

Fig. 4: Consensus controllers 3D trajectories of the UAV and UGV with two obstacles.

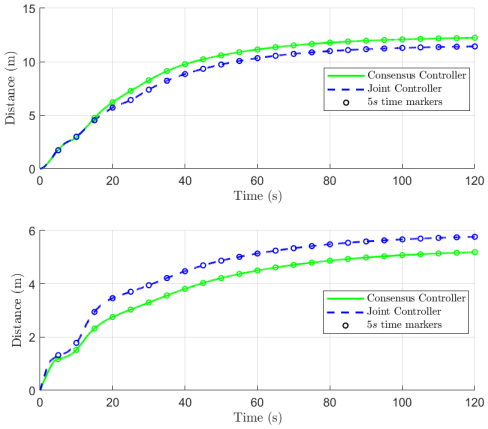

Fig. 5: Total distances traveled by UAV (top) and UGV (bottom).

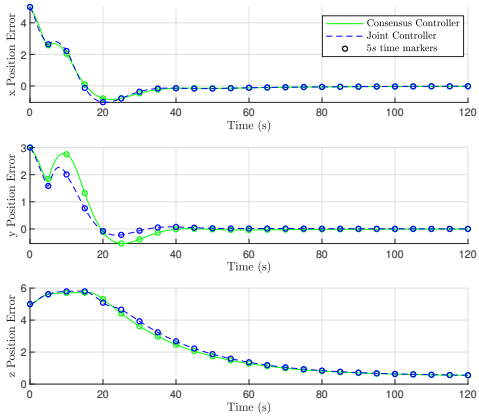

Fig. 6: Relative position errors between the UAV and UGV.

As can be seen in Fig. 6, the relative position errors converge to zero almost at the same time with both approaches. This is further confirmed in TABLE I where the landing time for both controllers is presented. Moreover, the total control effort from (24) is presented in TABLE I. The results indicate that the total control effort generated for the UGV is lower with the consensus controller while that generated for the UAV is slightly lower with the joint controller. It should be noted that this is affected by the tuning gains sensitivity.

C. Scenario 2: Three Obstacles

The effectiveness of the control approaches is further demonstrated when a third obstacle is added to the UAV path right before it fully lands. Both approaches are still capable of avoiding the obstacle and rendezvous as shown in Fig. 7 with the joint controller and Fig. 8 with the consensus controllers. The position errors are presented in Fig. 9 and TABLE II provides the performance metrics.

TABLE I: Scenario 1 Performance Metrics

Metric	Joint Controller	Consensus Controllers
Landing Time	159.72 s	159.88 s
Total Effort UGV	0.9680	0.6138
Total Effort UAV	0.9797	1.0767

V. Conclusion and Future Perspectives

This work presents the integration of obstacle avoidance to the UAV-UGV rendezvous problem with a desired rendezvous location. Two control approaches are presented, the first is an extension of a joint controller proposed in [10] through integrating obstacle avoidance for both vehicles (UGV and UAV) and forcing them to rendezvous at a predefined location. Meanwhile, the second approach is based on distributed consensus controllers with the same objective. The two approaches demonstrate similar behaviors, successfully avoiding obstacles and meeting at the desired location, while the second approach provides better scalability for the system. It should be noted that both approaches don't consider the physical limitations on the control inputs.

Therefore, future work aims to account for the physical limitations imposed by actuators and optimize the trade-off between convergence time and control effort. Furthermore, the extension of the system to include multiple UAVs and

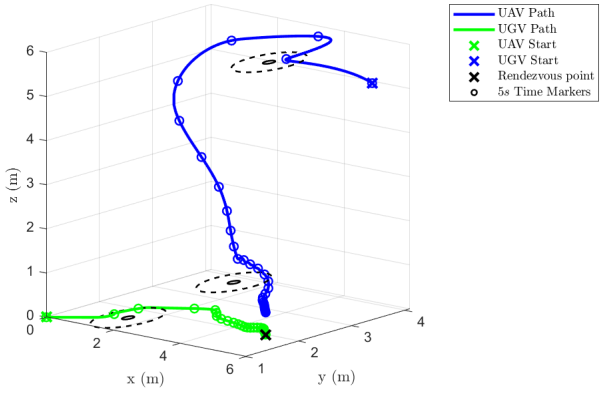

Fig. 7: Joint controller 3D trajectories of the UAV and UGV with three obstacles.

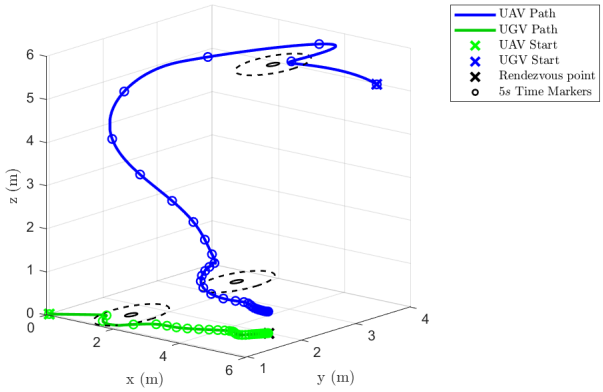

Fig. 8: Consensus controllers 3D trajectories of the UAV and UGV with three obstacles.

UGVs, working cooperatively, will be explored. Obstacle avoidance will also be further studied to allow the navigation through more complex environments.

REFERENCES

[1] A. B. Asghar, G. Shi, N. Karapetyan, J. Humann, J.-P. Reddinger, J. Dotterweich, and P. Tokekar, "Risk-aware Recharging Rendezvous for a Collaborative Team of UAVs and UGVs," in *2023 IEEE International Conference on Robotics and Automation (ICRA)*, (London, United Kingdom), pp. 5544–5550, May 2023.

[2] G. Niu, Q. Yang, Y. Gao, and M.-O. Pun, "Vision-Based Autonomous Landing for Unmanned Aerial and Ground Vehicles Cooperative Systems," *IEEE Robotics and Automation Letters*, vol. 7, pp. 6234–6241, July 2022.

[3] Y. Feng, C. Zhang, S. Baek, S. Rawashdeh, and A. Mohammadi, "Autonomous Landing of a UAV on a Moving Platform Using Model Predictive Control," *Drones*, vol. 2, p. 34, Oct. 2018.

[4] K. Guo, P. Tang, H. Wang, D. Lin, and X. Cui, "Autonomous Landing of a Quadrotor on a Moving Platform via Model Predictive Control," *Aerospace*, vol. 9, p. 34, Jan. 2022.

[5] G. Shi, N. Karapetyan, A. B. Asghar, J.-P. Reddinger, J. Dotterweich, J. Humann, and P. Tokekar, "Risk-aware UAV-UGV Rendezvous with Chance-Constrained Markov Decision Process," in *2022 IEEE 61st Conference on Decision and Control (CDC)*, (Cancun, Mexico), pp. 180–187, Dec. 2022.

[6] J. E. Ekoru, M. T. Ngwako, M. M. Madahana, and O. T. Nyandoro, "Singular optimal control for rendezvous problem for cooperative vehicle control," *IFAC-PapersOnLine*, vol. 56, pp. 3320–3325, July 2023.

[7] L. Persson, T. Muskardin, and B. Wahlberg, "Cooperative rendezvous of ground vehicle and aerial vehicle using model predictive control," in *2017 IEEE 56th Annual Conference on Decision and Control (CDC)*, (Melbourne, Australia), pp. 2819–2824, Dec. 2017.

[8] C. Hebisch, S. Jackisch, D. Moormann, and D. Abel, "Flatness-Based Model Predictive Trajectory Planning for Cooperative Landing on Ground Vehicles," in *2021 IEEE Intelligent Vehicles Symposium (IV)*, (Nagoya, Japan), pp. 1031–1036, July 2021.

[9] K. A. Ghamry, Y. Dong, M. A. Kamel, and Y. Zhang, "Real-time autonomous take-off, tracking and landing of UAV on a moving UGV platform," in *2016 24th Mediterranean Conference on Control and Automation (MED)*, (Athens, Greece), pp. 1236–1241, June 2016.

[10] J. M. Daly, Y. Ma, and S. L. Waslander, "Coordinated landing of a quadrotor on a skid-steered ground vehicle in the presence of time delays," *Autonomous Robots*, vol. 38, pp. 179–191, Feb. 2015.

[11] V. P. Bacheti, A. S. Brandao, and M. Sarcinelli-Filho, "A Path-Following Controller for a UAV-UGV Formation Performing the Final Step of Last-Mile-Delivery," *IEEE Access*, vol. 9, pp. 142218–142231, 2021.

[12] J. Guo, X. Dong, Y. Gao, D. Li, and Z. Tu, "Simultaneous Obstacles Avoidance and Robust Autonomous Landing of a UAV on a Moving Vehicle," *Electronics*, vol. 11, p. 3110, Sept. 2022.

[13] S. Piao, N. Li, and Z. Miao, "Research on UAV Vision Landing Target Detection and Obstacle Avoidance Algorithm," in *2023 42nd Chinese Control Conference (CCC)*, (Tianjin, China), pp. 4443–4448, July 2023.

[14] V. N. Sankaranarayanan, A. Saradagi, S. Satpute, and G. Nikolakopoulos, "Collision-Free Landing of Multiple UAVs on Moving Ground Vehicles Using Time-Varying Control Barrier Functions," in *2024 American Control Conference (ACC)*, (Toronto, ON, Canada), pp. 3760–3767, July 2024.

[15] A. Mohammadi and M. Bagher Menhaj, "Formation control and obstacle avoidance for nonholonomic robots using decentralized MPC," in *2013 10th IEEE International Conference on Networking, Sensing and Control (ICNSC)*, pp. 112–117, 2013.

[16] Z. H. Ismail and N. Sariff, "A survey and analysis of cooperative multi-agent robot systems: Challenges and directions," in *Applications of Mobile Robots* (E. G. Hurtado, ed.), ch. 1, Rijeka: IntechOpen, 2018.

[17] P. D. Kozłowski, Krzysztof, "Modeling and control of a 4-wheel skid-steering mobile robot," *International Journal of Applied Mathematics and Computer Science*, vol. 14, no. 4, pp. 477–496, 2004.

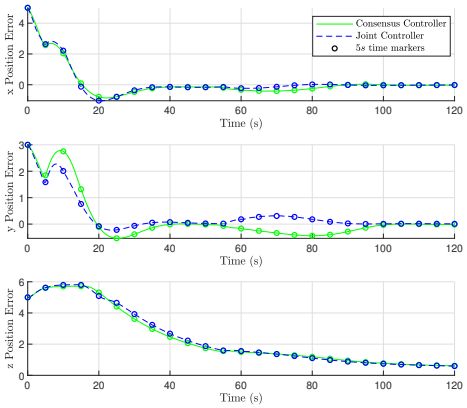

Fig. 9: Position errors between the UAV and UGV with three obstacles

TABLE II: Scenario 2 Performance Metrics

Metric	Joint Controller	Consensus Controllers
Landing Time	170.84 s	176.19
Total Effort UGV	0.9687	0.6121
Total Effort UAV	0.9908	1.0982